JOURNAL OF CHEMICAL & ENGINEERING DATA

ARTICLE

pubs.acs.org/jced

Thermodynamic Properties of 2,3,3,3-Tetrafluoroprop-1-ene (R1234yf): Vapor Pressure and $p-\rho-T$ Measurements and an Equation of State

Markus Richter,[†] Mark O. McLinden,* and Eric W. Lemmon

Thermophysical Properties Division, National Institute of Standards and Technology, 325 Broadway, Mailstop 838.07, Boulder, Colorado 80305, United States

Supporting Information

ABSTRACT: The $p-\rho-T$ behavior of 2,3,3,3-tetrafluoroprop-1-ene (R1234yf) was measured from T = (232 to 400) K with pressures up to 10 MPa using a two-sinker densimeter. The measurements extend from low-density vapor to compressed-liquid states, and include the extended critical region. Vapor pressures from T = (250 to 366) K were also measured. The expanded (k = 2) uncertainty in density is $(56 \cdot 10^{-6} \cdot \rho + 0.0014\ \mathrm{kg \cdot m^{-3}})$ at near-ambient conditions, increasing to $(99 \cdot 10^{-6} \cdot \rho + 0.0014\ \mathrm{kg \cdot m^{-3}})$ at T = 400 K and p = 10 MPa. The maximum uncertainties in temperature and pressure are 0.004 K and $(51 \cdot 10^{-6} \cdot p + 2.0\ \mathrm{kPa})$, respectively. The analysis for density accounts for the force transmission error in the magnetic suspension coupling of the densimeter and includes corrections for vertical density gradients in the measuring cell. These data, together with other data from the literature, have been used to develop an equation of state explicit in the Helmholtz energy covering the fluid region from T = (220 to 410) K with pressures up to 30 MPa. Comparisons to experimental data, including other literature data, are given to establish the accuracy of the equation of state.

1. INTRODUCTION

2,3,3,3-Tetrafluoroprop-1-ene (R1234yf) is a fluorinated hydrocarbon that has been recently proposed to replace R134a in automotive air-conditioning and other applications. R1234yf offers a remarkably low global warming potential (GWP) of 4 relative to CO_2 for a 100 year time horizon.[1] In comparison, R134a has a GWP of 1430. The atmospheric lifetime is 11 days compared to a lifetime for R134a of about 13 years.[1] Its short atmospheric lifetime is a result of the double bond in the chemical structure. The thermophysical properties of both fluids are similar, thus minimizing equipment changes in refrigeration applications. R1234yf has a critical temperature of 367.85 K.[2] Under normal conditions, it is a stable material of low toxicity, although it is slightly flammable. It has been assigned a safety classification of A2L according to ASHRAE Standard 34.[3]

In the present project, we have measured the $p-\rho-T$ properties and vapor pressures of R1234yf. These data, together with additional data from the literature, have been used to develop an equation of state covering the entire fluid region from T = (220 to 410) K with pressures up to 30 MPa. The present paper describes high-accuracy measurements of the $p-\rho-T$ behavior of high-purity (99.96 %) R1234yf from T = (232 to 400) K with pressures up to 10 MPa using a two-sinker densimeter; these include measurements in the vicinity of the critical point. Vapor pressures from T = (250 to 366) K were also measured. Detailed comparisons of the measured data with the new equation of state (EOS) and also with all prior literature data are given.

2. EXPERIMENTAL SECTION

For the measurements reported in this paper a two-sinker densimeter was utilized. This type of instrument applies the Archimedes (buoyancy) principle to provide an absolute determination of the density, that is, a measurement that is independent of calibration fluids. The accuracy of the Archimedes technique has been improved by the use of two sinkers. In particular, the two-sinker technique developed by Kleinrahm and Wagner[4] has proven very successful. The state of the art of this general type of instrument is described by Wagner and Kleinrahm.[5]

2.1. Apparatus Description. The two-sinker densimeter used in this work is described in detail by McLinden and Lösch-Will[6] as well as by Lösch-Will.[7] Only a brief description is given here. Two sinkers of nearly the same mass and surface area, but made of materials with different densities such that they have very different volumes, are weighed separately with a high-precision balance while they are immersed in a fluid of unknown density. For the present two-sinker densimeter, one sinker was made from tantalum with a mass m_1 of 60.177 91 g and a volume of 3.610 25 cm^3 at T = 293.15 K and ambient pressure, and the other was made from titanium with a mass m_2 of 60.163 34 g and a volume of 13.347 55 cm^3 at T = 293.15 K. The fluid density is given by

$$\rho_{\mathrm{fluid}} = \frac{(m_1 - m_2) - (W_1 - W_2)}{(V_1 - V_2)} \qquad (1)$$

where m and V are the sinker mass and volume, W is the balance reading, and the subscripts refer to the two sinkers.

Received: April 14, 2011
Accepted: May 21, 2011
Published: June 02, 2011

The main advantage of the two-sinker method is that adsorption onto the surfaces of the sinkers, systematic errors in the weighings, and other effects that reduce the accuracy of most buoyancy techniques largely cancel out. A magnetic suspension coupling (MSC) transmits the gravity and buoyancy forces on the sinkers to the balance, thus isolating the fluid sample (which may be at high pressure and high temperature) from the balance, which is placed under ambient conditions. The central elements of the coupling are two magnets, one on each side of a nearly nonmagnetic, pressure-separating wall. The top magnet, which is an electromagnet with a ferrite core, is attached to the under-pan weighing hook of the balance. The bottom (permanent) magnet is immersed in the fluid sample; it is held in stable suspension with respect to the top magnet by means of a feedback control circuit making fine adjustments in the electromagnet current. The permanent magnet is linked with a "lifting fork" to pick up a sinker for weighing. A mass comparator balance with a resolution of 1 μg and a capacity of 111 g is used for the weighings.

In addition to the sinkers, two calibration masses are also weighed. This calibrates the balance and provides the information needed to correct for magnetic effects as described by McLinden et al.[8] The weighings yield a set of four equations that are solved to yield a balance calibration factor α, a parameter β related to the balance tare (i.e., the magnets and other elements of the system that are always weighed), and a parameter ϕ, which expresses the efficiency of the MSC. This analysis yields the fluid density in terms of directly measured quantities:

$$\rho_{\text{fluid}} = \frac{\left[(m_1 - m_2) - \dfrac{(W_1 - W_2)m_1}{W_1 - \alpha\beta}\right]}{\left[(V_1 - V_2) - \dfrac{(W_1 - W_2)V_1}{W_1 - \alpha\beta}\right]} - \rho_0 \qquad (2)$$

where the ρ_0 is the indicated density when the sinkers are weighed in vacuum; ρ_0 accounts for small changes in sinker mass with time. The key point of the analysis by McLinden et al.[8] is that the density given by eq 2 compensates for the magnetic effects of both the apparatus and the fluid being measured. The effect of magnetic materials on the magnetic suspension coupling is known as the "force transmission error", and this effect is characterized by the coupling factor ϕ. A value of ϕ = 1 corresponds to a zero force transmission error; that is, the balance would give the same reading for an object weighed via the magnetic suspension coupling as for the same object weighed directly on the balance pan. For the present measurements ϕ varied from 1.000 022 in vacuum to 0.999 976 for R1234yf at the highest densities.

From the coupling factor ϕ and its variation with density it is possible to estimate the specific magnetic susceptibility of a fluid as detailed by McLinden et al.[8] R1234yf is slightly diamagnetic (as is typical for most fluids) with a specific magnetic susceptibility $\chi_s = -0.68 \cdot 10^{-8} \pm 0.12 \cdot 10^{-8}$ m$^3 \cdot$kg^{-1}.

In addition to the measuring cell, sinkers, suspension coupling, and balance that made up the density measuring system, the apparatus included a thermostat, pressure instrumentation, and a sample handling system. The temperature was measured with a 25 Ω standard platinum resistance thermometer (SPRT) and a resistance bridge referenced to a thermostatted standard resistor. The signal from the SPRT was used in a digital control circuit to maintain the cell temperature constant within ± 0.001 K. The pressures were measured with vibrating-quartz-crystal-type pressure transducers. One of three transducers, with maximum pressures of 2.80 MPa, 13.8 MPa, and 68.9 MPa, was used, depending on the pressure range. The transducers (as well as the pressure manifold) were thermostatted to minimize the effects of variations in laboratory temperature.

The thermostat isolated the measuring cell from ambient conditions. It was a vacuum-insulated, cryostat-type design. The measuring cell was surrounded by two isothermal shields. The first (inner) shield was directly attached to the measuring cell and was controlled to the same temperature. The second (outer) shield thermally isolated the measuring cell and the inner shield from variations in ambient temperature; this shield was maintained at a constant (± 0.01 K) temperature 1 K below the cell temperature by means of electric heating. Additional electric heaters on the cell compensated for the small heat flow from the cell to the shield and allowed millikelvin-level control of the cell temperature. Operation at subambient temperatures was effected by circulating ethanol from a chiller through channels in the outer shield.

2.2. Experimental Procedures. The measurements were carried out primarily along pseudoisochores (that is, varying temperature at states of nearly constant density). This procedure was used to minimize (compared to isothermal operation) the required quantity of sample. This also avoided the need to use any type of compressor, which is a possible source of contamination. The measuring cell was filled at a relatively high density and low temperature. After several replicate points were measured at the desired temperature, the cell was heated to the next, higher set-point temperature (thus raising the pressure), and measurements were made at that temperature. When measurements at the maximum temperature were completed, the cell was cooled, and a portion of the R1234yf charge was vented into a recovery bottle. The measurement of the next isochore then commenced. Two near-critical isotherms at T = 370 K and T = 380 K were also carried out.

The measurements comprised five separate fillings of R1234yf. The cell was evacuated between fillings (and also prior to the first filling and after the final filling), and measurements were carried out in vacuum to determine ρ_0. A fresh sample was used for each filling.

Vapor pressures were measured with the first filling of the cell, using the densimeter as a static vapor pressure instrument with the measuring cell partially filled with liquid (densities were not measured). In addition, check measurements of the vapor pressure were also carried out at the completion of several other fillings. The second filling studied the vapor phase densities; several replicate isochores were carried out with the fifth filling. Filling 3 was used to study compressed liquid-phase densities and also the supercritical isotherm at T = 370 K. The fourth filling measured supercritical states at T = 380 K.

2.3. Experimental Material. The supplier's analysis for the R1234yf indicated a purity of 99.96 %. Our own analysis by gas chromatography combined with mass spectrometry and infrared spectrophotometry (carried out according to the protocols of Bruno and Svoronos[9,10]) revealed only very small impurity peaks that were too small to permit identification. The sample was degassed by freezing in liquid nitrogen and evacuating the vapor space. The sample, as received, contained a considerable amount of dissolved air, and a total of eight freeze−pump−thaw cycles were carried out. On the final pumping cycle, the initial pressure in the vapor space was $1 \cdot 10^{-4}$ Pa. The material used in the densimeter was collected in a recovery bottle and analyzed again following the measurements; no change in the purity was detected.

Two different series of tests were performed to study the thermal stability of R1234yf. For the first set of tests, the fluid was heated for (16 to 23) h at T = 250 °C or at T = 150 °C in stainless steel ampule reactors with a volume of approximately 0.3 mL according to the protocols of Widegren and Bruno.[11] For the first two tests at T = 250 °C and T = 150 °C, the reactor was not evacuated prior to filling. Polymerization was observed in both cases. For the third test at T = 150 °C, the reactor was thoroughly evacuated prior to filling, and no polymerization was detected. Thus, air promotes the polymerization of R1234yf. For the second set of tests, a pressure vessel of type 316 stainless steel with a volume of about 16 mL was used; here shavings of copper−beryllium, titanium, tantalum, stainless steel, and gold-plated copper were placed in the test reactor to include any possible interactions between the fluid and the materials of the densimeter. Before filling the reactor, it was evacuated to a pressure of about $1 \cdot 10^{-4}$ Pa. The reactor was weighed and completely filled with the R1234yf. To obtain the desired maximum pressure at the test temperature, the mass of the sample was appropriately vented. After weighing the test reactor again, it was put into an oven for 72 h (first test at T = 150 °C and p = 20 MPa, second test at T = 120 °C and p = 12 MPa, and third test at T = 120 °C and p = 6 MPa). Polymerization was observed for the first two tests but not in the third. Thus high pressure as well as high temperature promotes polymerization of R1234yf. These tests served to determine the maximum temperature and pressure of the subsequent measurements.

3. RESULTS

3.1. Uncertainty of the Measurements. The experimental uncertainties of the individual properties p, ρ, and T have been discussed in detail in previous papers.[6,12] The expanded uncertainty (k = 2, or approximately 95 % confidence level) in density is given by

$$\frac{u(\rho)}{\mathrm{kg \cdot m^{-3}}} = \left\{ (56)^2 + \left[0.75 \left(\frac{T}{\mathrm{K}} - 293 \right) \right]^2 + \left(1.25 \frac{p}{\mathrm{MPa}} \right)^2 \right\}^{0.5} \frac{10^{-6} \rho}{\mathrm{kg \cdot m^{-3}}} + 0.0014 \quad (3)$$

This uncertainty in density accounts for the uncertainties in the weighings, the sinker volumes, and the force transmission error in the magnetic suspension coupling of the densimeter; it also includes corrections for vertical density gradients in the measuring cell. A detailed description of the force transmission error analysis of the NIST two-sinker densimeter is given by McLinden et al.[8] The temperature reported in the $p-\rho-T$ data was determined with the measuring-cell standard platinum resistance thermometer (SPRT), which was calibrated on ITS-90 by using fixed-point cells in the temperature range from (83 to 505) K (argon triple point, mercury triple point, water triple point, indium freezing point, and tin freezing point). The expanded uncertainty (k = 2) in the temperature is 4 mK. Pressures are measured with three different transducers, which were calibrated by use of a piston gauge. The expanded uncertainty (k = 2) of the pressure measurement is $(40 \cdot 10^{-6} \cdot p + 0.06$ kPa) for the low-range transducer, $(40 \cdot 10^{-6} \cdot p + 0.30$ kPa) for the midrange transducer, and $(52 \cdot 10^{-6} \cdot p + 2.0$ kPa) for the high-range transducer.

Table 1. Experimental Vapor Pressure p_{sat} for R1234yf from T = (250 to 366) K and Relative Deviations of the Experimental Data from Values Calculated with the New Equation of State Developed in this Work Δ_p[a]

T/K	p_{sat}/MPa	Δ_p
	Filling 1	
269.998	0.28341	−0.0021
279.999	0.39591	0.0004
290.000	0.53938	0.0085
250.002	0.13337	0.4770
260.003	0.19744	0.1271
270.005	0.28348	−0.0139
290.002	0.53942	0.0088
299.999	0.71868	−0.0029
309.999	0.93928	−0.0114
311.999	0.98909	0.0107
314.000	1.04087	0.0328
315.999	1.09440	0.0343
320.000	1.20763	0.0361
330.001	1.52905	0.0350
340.002	1.91025	−0.0110
350.003	2.36144	−0.0032
355.004	2.61653	0.0055
360.005	2.89380	0.0137
362.005	3.01152	0.0162
364.005	3.13357	0.0165
366.005	3.26023	0.0101
309.999	0.93930	−0.0073
320.000	1.20765	0.0360
	Filling 3	
319.994	1.20704	0.0017
	Filling 4	
319.994	1.20638	−0.0535
	Filling 5	
250.000	0.13303	0.2310
270.000	0.28303	−0.1405
289.995	0.53895	−0.0581
309.989	0.93857	−0.0612
319.990	1.20681	−0.0095

[a] Only one point per temperature T is given; see Supporting Information for all data.

The variance in the multiple measurements of temperature and pressure carried out during the course of a single density determination was added (in quadrature) to the above instrument uncertainties. The variance in the multiple balance readings constituting a density determination was converted to their equivalent effect on density and added to the density uncertainty given by eq 3. In most cases these variances (or "type A" uncertainties) are small compared to the systematic (or "type B") uncertainties arising from instrument calibrations and other effects. These are detailed for each measured point in the Supporting Information. An additional pressure uncertainty, amounting to (0.1 to 0.35) kPa, was added to the vapor pressure data to reflect an increased uncertainty in the hydrostatic head correction.

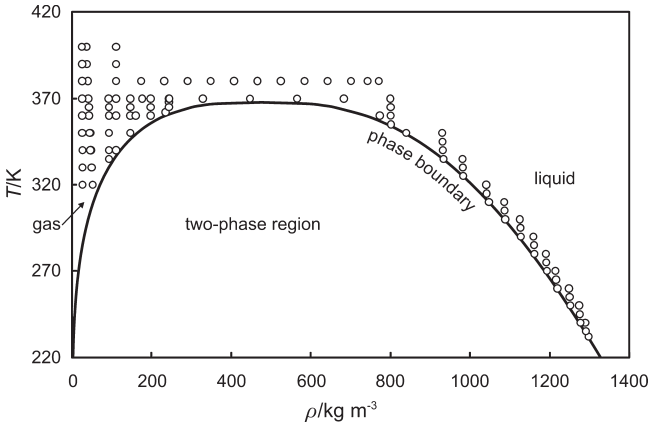

Figure 1. $p-\rho-T$ state points measured for R1234yf in the present work.

The above uncertainties for temperature, pressure, and density are for these quantities in isolation. For the purpose of fitting an equation of state, it is customary to assume that the temperature and pressure (or sometimes temperature and density) are known exactly, and lump all uncertainties into a single value for the density (or pressure). This overall combined, or state-point, uncertainty is given by

$$u_C(\rho) = \left\{ [u(\rho)]^2 + \left[\left(\frac{\partial \rho}{\partial p} \right)_T u(p) \right]^2 + \left[\left(\frac{\partial \rho}{\partial T} \right)_p u(T) \right]^2 \right\}^{0.5} \quad (4)$$

where u_C designates a combined uncertainty, u stands for the individual uncertainties, and the derivatives are calculated with an equation of state. For near-critical states where deviations in pressure are an appropriate measure of quality (as discussed by McLinden[12]), the state-point uncertainty is

$$u_C(p) = \left\{ [u(p)]^2 + \left[\left(\frac{\partial p}{\partial \rho} \right)_T u(\rho) \right]^2 + \left[\left(\frac{\partial p}{\partial T} \right)_\rho u(T) \right]^2 \right\}^{0.5} \quad (5)$$

For vapor pressure, the combined uncertainty can be calculated with

$$u_C(p_{sat}) = \left\{ [u(p)]^2 + \left[\left(\frac{\partial p_{sat}}{\partial T} \right) u(T) \right]^2 \right\}^{0.5} \quad (6)$$

These state-point uncertainties are tabulated for each measured point in the Supporting Information.

3.2. Vapor Pressures. The densimeter was used to measure the vapor pressure of R1234yf at 28 temperatures from $T = (250$ to $366)$ K. Four to eight replicate determinations were carried out at each temperature to yield 216 data points. The experimental data are given in Table 1, and deviations to the equation of state developed within this work are given by

$$\Delta_p = 100 \left(\frac{p_{exp} - p_{EOS}}{p_{EOS}} \right) \quad (7)$$

Only average values of the replicates are reported in the table at

Table 2. Experimental $p-\rho-T$ Data for R1234yf and Relative Deviations of the Experimental Data from Densities Calculated with the New Equation of State Developed in this Work Δ_ρ[a]

T/K	p/MPa	ρ/kg·m^{-3}	Δ_ρ
		Filling 2	
368.002	3.1843	243.231	−0.0208
370.003	3.2486	243.253	0.0086
362.001	2.9637	235.115	0.1425
365.002	3.0867	243.237	−0.0698
360.003	2.7679	197.534	−0.0983
365.005	2.8926	197.483	−0.0059
370.003	3.0149	197.482	0.0743
350.000	2.2619	146.580	−0.1557
360.002	2.4336	146.594	−0.0008
365.003	2.5167	146.549	0.0620
370.004	2.5985	146.499	0.1205
334.999	1.5925	92.726	−0.1163
339.998	1.6405	92.612	−0.0731
350.000	1.7368	92.623	−0.0022
360.002	1.8305	92.622	0.0553
365.003	1.8766	92.619	0.0805
370.007	1.9205	92.497	0.1052
329.998	0.9859	49.464	−0.0260
339.999	0.9935	47.298	−0.0104
350.000	1.0030	45.555	0.0124
360.002	1.0052	43.637	−0.0344
365.002	0.9919	42.073	−0.0421
370.003	0.9963	41.436	−0.0444
		Filling 3	
232.010	1.0036	1297.663	0.0166
235.007	1.3544	1290.571	0.0137
240.007	5.5979	1288.716	0.0074
240.008	1.3097	1276.935	0.0104
245.004	5.3687	1275.086	0.0040
250.001	9.4752	1273.530	0.0002
250.004	2.0093	1251.504	0.0013
255.003	5.7827	1249.792	−0.0018
260.001	9.5862	1248.324	−0.0025
260.002	1.0014	1219.361	−0.0042
265.000	3.8247	1215.480	−0.0059
270.000	7.2648	1214.106	−0.0039
270.002	1.7533	1192.465	−0.0089
275.000	4.9311	1190.995	−0.0054
280.000	8.1234	1189.714	0.0009
279.999	1.7809	1161.426	−0.0101
284.998	4.6759	1160.065	−0.0013
289.998	7.5791	1158.847	0.0082
289.999	1.6048	1127.358	−0.0088
294.997	4.1986	1126.002	0.0047
299.998	6.8121	1124.848	0.0181
299.997	1.0792	1087.768	−0.0110
304.995	3.3643	1086.434	0.0090
309.994	5.6739	1085.352	0.0271
309.995	1.0040	1047.051	−0.0184

dx.doi.org/10.1021/je200369m |J. Chem. Eng. Data 2011, 56, 3254–3264

Table 2. Continued

T/K	p/MPa	ρ/kg·m^{-3}	Δ_ρ
314.994	2.5117	1041.014	0.0026
320.000	4.5180	1040.051	0.0286
325.001	1.4563	982.689	−0.0529
330.001	3.1082	981.791	−0.0023
335.002	4.7708	980.976	0.0336
335.002	1.7980	932.524	−0.0772
340.002	3.1915	931.599	−0.0080
345.003	4.5941	930.707	0.0351
350.004	6.0054	929.873	0.0591
350.004	2.4610	839.342	−0.0372
355.001	2.7403	801.182	−0.0129
360.002	3.6388	800.559	0.0073
365.003	4.5537	799.933	0.0210
370.003	5.4807	799.340	0.0253
370.002	3.2522	244.129	−0.0131
370.002	2.8668	176.561	0.0878
		Filling 4	
360.000	3.2105	772.483	−0.0117
380.004	6.5832	770.356	0.0067
380.005	3.4961	231.990	0.1678
380.004	3.0473	173.864	0.2220
360.001	2.5454	160.529	−0.0381
		Filling 5	
339.998	1.8278	110.941	−0.1714
360.000	2.0670	110.845	0.0311
370.001	2.1816	110.789	0.1030
380.002	2.2939	110.737	0.1636
390.003	2.4041	110.680	0.2151
400.004	2.5129	110.640	0.2579
319.995	0.9732	51.726	−0.0433
329.995	0.9792	49.047	−0.0235
339.996	0.9809	46.550	−0.0629
349.997	0.9859	44.652	0.0340
359.998	0.9872	42.763	0.0165
370.000	0.9937	41.326	−0.0113
380.000	0.9948	39.809	−0.0178
390.001	0.9878	38.088	−0.0366
400.002	0.9914	36.952	−0.0414
319.994	0.5539	26.402	−0.0371
329.994	0.5740	26.306	−0.0314
339.995	0.5938	26.211	−0.0290
349.996	0.6132	26.120	−0.0273
359.998	0.6324	26.029	−0.0282
369.999	0.6512	25.938	−0.0290
380.000	0.6679	25.765	−0.0341
390.001	0.6707	25.062	−0.0157
400.002	0.6832	24.785	−0.0012

[a] Data are along pseudo-isochores and are presented in the sequence measured. Only one point per temperature−pressure (T, p) state point is given; see Supporting Information for all data.

each temperature; all of the data points are included in the Supporting Information. The data are compared to other literature data and the new EOS in section 4.2.

Table 3. Experimental $p-\rho-T$ Data for R1234yf in the Near-Critical Region ($285 < \rho/\text{kg·m}^{-3} < 761$) and Relative Deviations of the Experimental Data from Pressures Calculated with the Equation of State Developed in this Work Δ_p[a]

T/K	p/MPa	ρ/kg·m^{-3}	Δ_ρ
		Filling 3	
370.003	3.8720	682.810	0.1035
370.002	3.5652	564.956	−0.0301
370.002	3.5225	447.008	0.0100
370.002	3.4535	328.135	0.0238
		Filling 4	
380.004	5.9861	742.567	−0.0122
380.005	5.3433	700.635	0.0010
380.005	4.8029	642.277	0.0214
380.004	4.5049	583.708	0.0113
380.004	4.3294	524.756	−0.0035
380.004	4.2074	465.809	0.0052
380.004	4.0977	407.116	0.0253
380.004	3.9677	348.398	0.0227
380.004	3.7828	290.103	−0.0101

[a] Data are along isotherms, and only one point per temperature−pressure (T, p) state point is given; see Supporting Information for all data.

3.3. $p-\rho-T$ Data in the Liquid and Vapor Phases. Densities of R1234yf were measured at 106 (T, p) state points at temperatures from T = (232 to 400) K with pressures up to 10 MPa. Four to eight replicates were measured at each state point for a total of 557 $p-\rho-T$ data. The measured points are depicted in Figure 1.

Our measured data are presented in Tables 2 and 3. Also reported are the relative deviations with the values calculated by the equation of state developed in this work:

$$\Delta_\rho = 100\left(\frac{\rho_{\text{exp}} - \rho_{\text{EOS}}}{\rho_{\text{EOS}}}\right) \quad (8)$$

The values listed in these tables present an average of the replicate measurements at a given (T, p) state. All of the measured data are available in the Supporting Information. The experimental temperatures and pressures are averages of the readings taken over the 12 min needed to complete a single density determination. Detailed comparisons with all of the available literature data are presented in section 4.2.

3.4. Correction for Density Gradients and $p-\rho-T$ Data in the Extended Critical Region. Equation 2 assumes that the fluid density is the same for all the weighings needed for a single density determination and, in particular, that both sinkers sense the same density. The two sinkers are located one above the other in the measuring cell and will thus experience different densities because of hydrostatic pressure gradients. In most cases, this correction is negligible. Near the critical point, however, the compressibility becomes large, and this effect can become significant. For measurements in the extended critical region ($285 < \rho/\text{kg·m}^{-3} < 761$), values of the coupling factor ϕ are obtained by fitting ϕ outside the critical region as a linear

Table 4. Summary of Experimental Data Considered in the Present Equation of State Fit for R1234yf Giving Experimental Ranges and Uncertainties[a]

author	no. of points	sample purity	range of T	range of p	range of ρ	uncertainty[b]
		mol %	K	MPa	kg·m^{-3}	
			Critical Parameters			
Hulse et al.[19c]	1	n.s.	367.95			0.2 K
Tanaka and Higashi[2]	1	99.99	367.85		487	0.01 K, 3 kg·m^{-3}
			Ideal-Gas Isobaric Heat Capacity			
Hulse et al.[19c]	13	n.a. (calc.)	213 to 573			n.s.
Kano et al.[18]	4	99.9	278 to 323			0.1 %
Kazakov[20]	n.a.	n.a. (calc.)	200 to 600			n.s.
			Vapor Pressure			
present work	216	99.96	250 to 366	0.13 to 3.1		4 mK, (0.20 to 0.55) kPa
DiNicola et al.[16]	35	99.95	224 to 366	0.039 to 3.2		0.02 K, 1 kPa
Fedele et al.[23c]	20	99.5	246 to 343	0.11 to 2.0		0.03 K, 1 kPa
Hulse et al.[19c]	12	n.s.	241 to 353	0.088 to 2.4		0.10 K, 0.25 %
Tanaka and Higashi[2]	11	99.99	310 to 360	0.94 to 2.9		5 mK, 1 kPa
			Saturated Liquid Density			
Hulse et al.[19]	9	n.s.	265 to 365		650 to 1200	0.01 K, 0.2 kg·m^{-3}
Tanaka and Higashi[2]	9	99.99	348 to 368		484 to 848	5 mK, 1.7 kg·m^{-3}
			Saturated Vapor Density			
Tanaka and Higashi[2c]	12	99.99	356 to 368		196 to 438	5 mK, 1.7 kg·m^{-3}
			Density as $f(T,p)$			
present work	557	99.96	232 to 400	0.55 to 9.6	41 to 1298	4 mK, (0.3 to 2.0) kPa, (0.006 to 0.012) %
DiNicola et al.[14c]	136	99.95	243 to 373	0.084 to 3.7	5.0 to 456	0.020 K, 0.8 %, 0.8 %
Tanaka et al.[15]	23	99.99	310 to 360	1.0 to 5.0	752 to 1081	5 mK, 3 kPa, 0.2 %
			Speed of Sound			
Lago et al.[17]	22	99.99	260 to 360	2.0 to 6.1		0.03 K, 0.1 MPa, (0.077 to 0.23) %
Kano et al.[18]	28	99.9	278 to 323	0.025 to 0.40		4 mK, 1 kPa, 0.01 %
			Isobaric Heat Capacity			
Tanaka et al.[15c]	22	99.99	310 to 360	2.0 to 5.0		5 mK, 3 kPa, 5 %

[a] n.a.: not applicable (values from theoretical calculation); n.s.: not stated. [b] Uncertainties are those indicated by the author and are listed in the order: T, p, (ρ or other dependent variable). [c] Data set not used in the equation of state fit.

function of density. This point is discussed in detail by McLinden.[12]

4. EQUATION OF STATE

A 15-term equation of state for R1234yf was fitted with the Helmholtz energy as the fundamental property with independent variables of density and temperature. The fit started with the "short form" equation of state of Span and Wagner;[13] the final EOS is a related, but more flexible form. For its development, the present measured vapor pressures, densities, and critical-region data plus additional $p-\rho-T$ data,[2,14,15] vapor pressures,[2,16] speed of sound data,[17,18] and isobaric heat capacities[15,18−20] were used. The data considered here are summarized in Table 4. The equation of state is valid from T = (220 to 410) K and for pressures up to 30 MPa.

4.1. Form of the Equation of State. The equation of state is given by

$$a(\rho, T) = a^0(\rho, T) + a^r(\rho, T) \qquad (9)$$

where a is the Helmholtz energy, $a^0(\rho,T)$ designates the ideal gas contribution to the Helmholtz energy, and $a^r(\rho,T)$ is the residual Helmholtz energy, which accounts for the influence of intermolecular forces. All thermodynamic properties can be calculated as derivatives of the Helmholtz energy. The functional form is explicit in the dimensionless Helmholtz energy, α, using independent variables of dimensionless density and temperature. The form of this equation is

$$\frac{a(\rho, T)}{RT} = \alpha(\delta, \tau) = \alpha^0(\delta, \tau) + \alpha^r(\delta, \tau) \qquad (10)$$

where R is the molar gas constant, $\delta = \rho/\rho_c$, $\tau = T_c/T$, the critical temperature is T_c = 367.85 K (ITS-90), and the critical density is ρ_c = 4.17 mol·dm^{-3} ($\approx$ 475.55 kg·m^{-3}). The critical pressure is p_c = 3382.2 kPa. The critical temperature of Tanaka and Higashi[2] is adopted in this work, while the values of ρ_c and p_c result from the fitting process. The molar mass of R1234yf is 114.04159 g·mol^{-1}. (Although this number of significant digits is not physically justified, it is important to retain all the digits when programming the equation.) The ideal gas Helmholtz

dx.doi.org/10.1021/je200369m |J. Chem. Eng. Data 2011, 56, 3254–3264

Table 5. Values for v_i and u_i in eq 12

i	v_i	u_i
1	7.549	718.0
2	1.537	877.0
3	2.030	4465.0
4	7.455	1755.0

energy can be written in a dimensionless form as

$$\alpha^0 = \frac{h_0^0\tau}{RT_c} - \frac{s_0^0}{R} - 1 + \ln\frac{\delta\tau_0}{\delta_0\tau} - \frac{\tau}{R}\int_{\tau_0}^{\tau}\frac{c_p^0}{\tau^2}d\tau + \frac{1}{R}\int_{\tau_0}^{\tau}\frac{c_p^0}{\tau}d\tau \quad (11)$$

where $\delta_0 = \rho_0/\rho_c$ and $\tau_0 = T_c/T_0$, and T_0, ρ_0, h_0^0, and s_0^0 are used to define an arbitrary reference state. The equation for the ideal gas heat capacity was fitted to measured and calculated c_p^0 values[18−20] and is given by

$$\frac{c_p^0}{R} = 5.944 + \sum_{i=1}^{4} v_i\left(\frac{u_i}{T}\right)^2\frac{\exp(u_i/T)}{[\exp(u_i/T)-1]^2} \quad (12)$$

where the values for v_i and u_i determined in this work are given in Table 5, and the gas constant, R, is 8.314472 J·mol^{-1}·K^{-1} (Mohr et al.[21]). A more convenient form of the ideal gas Helmholtz energy, derived from the integration of eq 11 and the application of a reference state with the enthalpy equal to 200 kJ·kg^{-1} and entropy equal to 1 kJ·kg^{-1}·K^{-1} for the saturated liquid at 0 °C, is

$$\alpha^0 = a_1 + a_2\tau + \ln\delta + 4.944\ln\tau + \sum_{i=1}^{4} v_i\ln[1-\exp(-u_i\tau/T_c)] \quad (13)$$

where $a_1 = -12.837928$ and $a_2 = 8.042605$.

The functional form for the residual Helmholtz energy is

$$\alpha^r(\delta,\tau) = \sum_{k=1}^{5} N_k\tau^{t_k}\delta^{d_k} + \sum_{k=6}^{10} N_k\tau^{t_k}\delta^{d_k}\exp(-\delta^{l_k}) + \sum_{k=11}^{15} N_k\tau^{t_k}\delta^{d_k}\exp[-\eta_k(\delta-\varepsilon_k)^2 - \beta_k(\tau-\gamma_k)^2] \quad (14)$$

where the coefficients and exponents determined in this work are given in Table 6. This equation is valid from T = (220 to 410) K. Due to constraints imposed in the fitting process, the equation should extrapolate well to the triple-point temperature and to higher temperatures, although with increased uncertainties. The equations used to calculate pressure, enthalpy, heat capacity, speed of sound, and so forth, from the equation of state are given by Lemmon et al.[22]

4.2. Comparisons with the Data. The equation of state was mainly fitted to the high-accuracy data measured within the present project but also made use of data from other authors.[2,14−20] Comparisons of the equation of state with experimental data are presented below. The quality of the fit is expressed in terms of the relative standard deviation defined here as

$$\sigma = \{\sum_{i=1}^{n}[100(z_{exp,i} - z_{EOS,i})/z_{EOS,i}]^2/(n-1)\}^{0.5} \quad (15)$$

where z is the property, and n is the number of data points used for the comparison. The term given in the brackets of the numerator of eq 15 is the relative deviation.

Table 6. Coefficients and Exponents of the Equation of State (eq 14)

k	N_k	t_k	d_k	l_k	η_k	β_k	γ_k	ε_k
1	0.04592563	1.0	4					
2	1.546958	0.32	1					
3	−2.355237	0.929	1					
4	−0.4827835	0.94	2					
5	0.1758022	0.38	3					
6	−1.210006	2.28	1	2				
7	−0.6177084	1.76	3	2				
8	0.6805262	0.97	2	1				
9	−0.6968555	2.44	2	2				
10	−0.02695779	1.05	7	1				
11	1.389966	1.4	1	-	1.02	1.42	1.13	0.712
12	−0.4777136	3.0	1	-	1.336	2.31	0.67	0.910
13	−0.1975184	3.5	3	-	1.055	0.89	0.46	0.677
14	−1.147646	1.0	3	-	5.84	80.0	1.28	0.718
15	0.0003428541	3.5	2	-	16.2	108.0	1.20	1.640

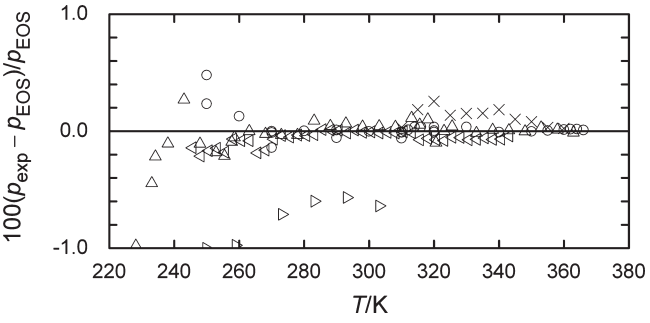

Figure 2. Relative deviations of the experimental vapor pressures p_{exp} for R1234yf from values calculated with the present equation of state p_{EOS}; ○, present work; △, Di Nicola et al. (2010); right-pointing triangle, Hulse et al.;[19] ×, Tanaka and Higashi;[2] left-pointing triangle, Fedele et al.[23]

Relative deviations between measured vapor pressures and values calculated from the new equation of state are depicted in Figure 2. The present data are represented with a relative standard deviation of 0.11 %. For temperatures above T = 270 K, the relative standard deviation decreases to 0.06 %. The data of Hulse et al.[19] show relative deviations of up to −2.89 %. The vapor pressures of Di Nicola et al.[16] are in excellent agreement with the present data except at temperatures below T = 260 K where the deviations increase to −1.32 %. Tanaka and Higashi[2] measured vapor pressures at temperatures of T = 310 K and higher, and their data are in very good agreement with the present data. They have a relative standard deviation of 0.07 %. The data of Fedele et al.[23] were received too late to be included in the fit, but they are, nevertheless, well-represented by the EOS, with a relative standard deviation of 0.06 %.

The $p-\rho-T$ data measured here are compared with the new equation of state in Figure 3, where the relative deviations between measured values and values calculated from the equation are plotted as a function of density ρ (a), as a function of temperature T (b), and as a function of pressure p (c). The

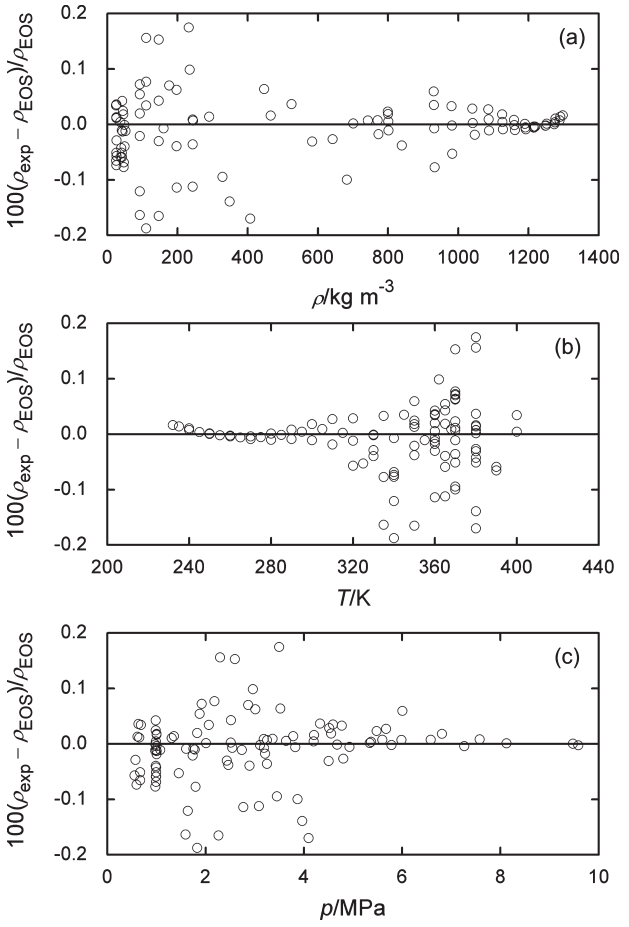

Figure 3. Relative deviations of the experimental densities ρ_{exp} for R1234yf from values calculated with the present equation of state ρ_{EOS}; (a) plotted as a function of density ρ; (b) plotted as a function of temperature T; (c) plotted as a function of pressure p; ○, present work.

measured data agree very well with the new equation of state; in the vicinity of the critical point (T_c = 367.85 K, p_c = 3.3822 MPa, and $\rho_c \approx$ 475.55 kg·m^{-3}), the scatter is larger than in the homogeneous liquid and gas regions. The present data have a relative standard deviation of 0.08 %.

Figure 4 shows deviation plots of $p-\rho-T$ data as a function of pressure p for six different temperature ranges for both the present data and the data from the literature. By means of Figure 4 it can be clearly stated that the data measured in this work are the most comprehensive. They also show the smallest deviations from the equation of state in all of the illustrated temperature ranges. The data of Tanaka et al.[15] are also in excellent agreement with the new equation of state, but their $p-\rho-T$ data were measured over the limited temperature range from T = (300 to 360) K at pressures between (1 and 5) MPa. A large data set for temperatures from T = (243 to 373) K at pressures to 3.7 MPa (but mainly at pressures below 1 MPa) was published by Di Nicola et al.[14] These data show the largest scatter as well as the largest deviations.

Data measured in the near-critical region (285 < ρ/kg·m^{-3} < 761) are compared in terms of deviations between the measured pressure and the pressure calculated from the equation of state as a function of temperature T, as plotted in Figure 5. The relative standard deviation in pressure p of the present data is 0.03 %.

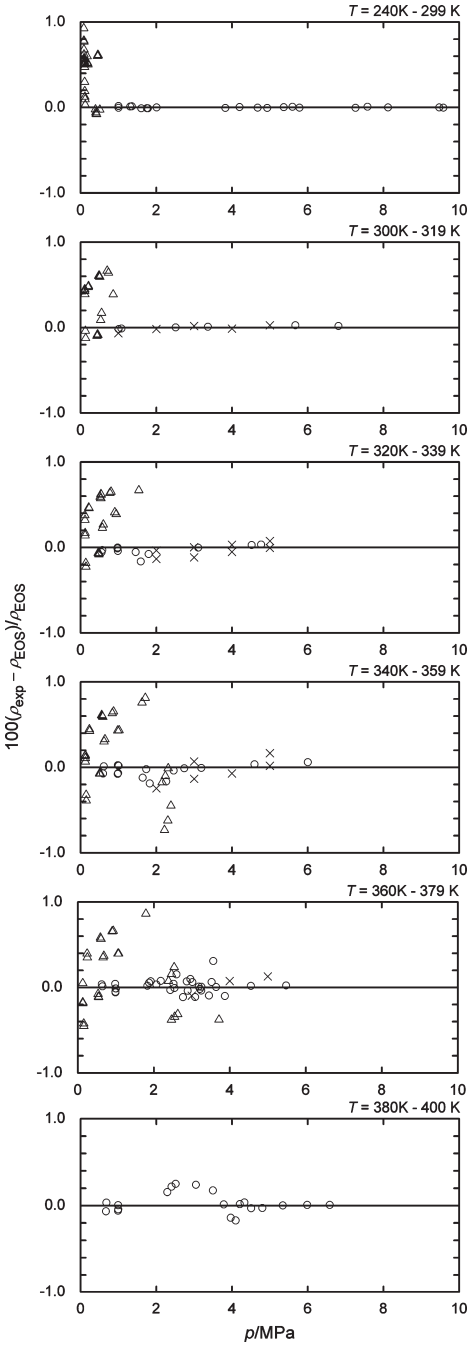

Figure 4. Relative deviations of the experimental densities ρ_{exp} for R1234yf from values calculated with the present equation of state ρ_{EOS} plotted as a function of pressure p; ○, present work; △, Di Nicola et al. (2010); ×, Tanaka et al.[15]

Only the present work provides experimental data in this particular fluid region of R1234yf.

Saturated-liquid and saturated-vapor densities have been measured by Tanaka and Higashi[2] and Hulse et al.[19] For the saturated liquid-densities, comparisons with the equation of state are given in Figure 6, and for the saturated-vapor densities in Figure 7. Measured saturated-liquid densities are represented by the equation with a relative standard deviation of 0.82 %. Saturated-vapor densities have a relative standard deviation of 2.57 % with the equation. The saturated-vapor densities were not used in the fit because of their higher uncertainty.

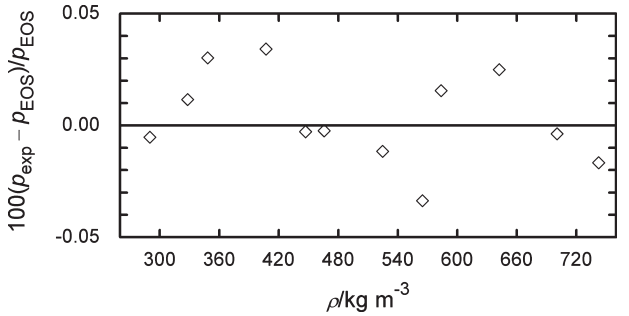

Figure 5. Relative deviations of experimental near-critical $p-\rho-T$ data points for R1234yf from values calculated with the present equation of state plotted as a function of density ρ; the deviations in pressure are plotted; ◊, present work (near-critical data).

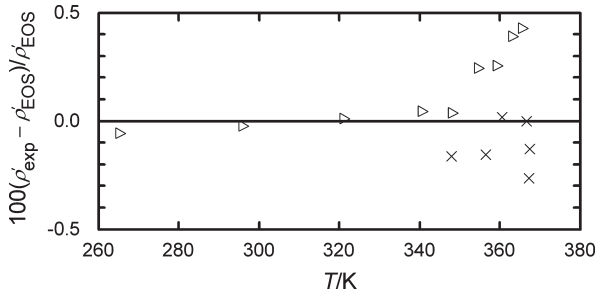

Figure 6. Relative deviations of the experimental saturated-liquid densities ρ'_{exp} for R1234yf from values calculated with the present equation of state ρ'_{EOS} plotted as a function of temperature; right-pointing triangle, Hulse et al.;[19] ×, Tanaka and Higashi.[2]

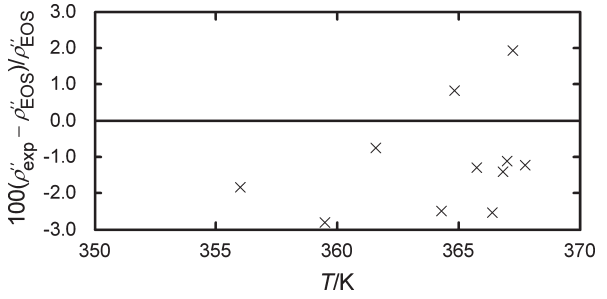

Figure 7. Relative deviations of the experimental saturated-vapor densities ρ''_{exp} for R1234yf from values calculated with the present equation of state ρ''_{EOS} plotted as a function of temperature; ×, Tanaka and Higashi.[2]

The comparisons of isobaric heat capacities at both ideal-gas and real-gas states with the equation of state are depicted in Figures 8 and 9, respectively. Hulse et al.[19] calculated ideal gas isobaric heat capacities over a large temperature range from T = (213.15 to 573.15) K with a relative standard deviation of 0.25 %. However, they show bias errors ranging between 0.83 % and 1.49 %. Kazakov[20] used predictive techniques to estimate the ideal gas heat capacity of this fluid. The c_p^0 data of Kano et al.,[18] which were derived from speed of sound measurements, are in good agreement with the final equation with a relative standard deviation of 0.29 %. Although the Kano et al. data covered a limited temperature range they verified that the predictions of Kazakov were quite good. Liquid phase isobaric heat capacities

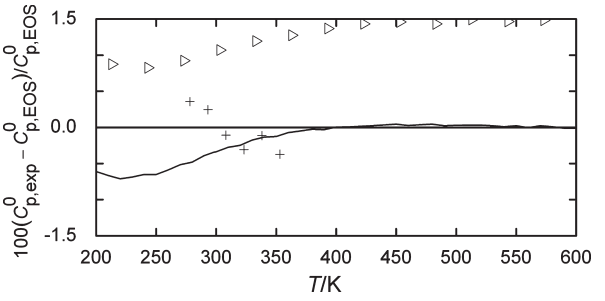

Figure 8. Relative deviations of the experimental ideal-gas isobaric heat capacities $c^0_{p,exp}$ for R1234yf from values calculated with the present equation of state $c^0_{p,exp}$ plotted as a function of temperature; +, Kano et al.;[18] right-pointing triangle, Hulse et al.;[19] —, Kazakov.[20]

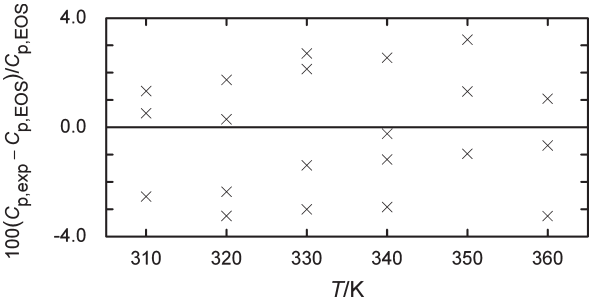

Figure 9. Relative deviations of the experimental liquid-phase isobaric heat capacities $c_{p,exp}$ for R1234yf from values calculated with the present equation of state $c_{p,exp}$ plotted as a function of temperature; ×, Tanaka et al.[15]

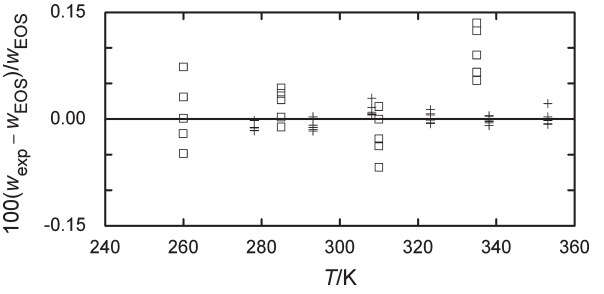

Figure 10. Relative deviations of the experimental speed of sound w_{exp} for R1234yf from values calculated with the present equation of state w_{EOS} plotted as a function of temperature; +, Kano et al. (vapor phase);[18] □, Lago et al. (liquid phase).[17]

have only been measured by Tanaka et al.,[15] with an estimated uncertainty of 5 %. The scatter of their data is large and has a relative standard deviation of 2.25 %.

Speed of sound data were also used to fit the new equation of state. Comparisons between the measured values in the liquid phase by Lago et al.[17] and in the vapor phase by Kano et al.[18] against values calculated from the new equation are illustrated in Figure 10. The vapor phase data of Kano et al.[18] are represented with a relative standard deviation of 0.01 %. These high-accuracy data were useful in the determination of the ideal gas heat capacity equation. After the completion of the equation of state, we obtained the data of Yoshitake et al.[24] for the liquid phase speed of sound; these data differ by about 0.75 % from the data of Lago et al.[17] It is unclear which measurements are more correct,

and additional experiments should be performed to aid in this evaluation.

The expanded uncertainty (k = 2, corresponding to an approximate 95 % confidence interval) in the density of the equation of state is 0.1 % in the liquid from T = (240 to 320) K and pressures up to 10 MPa. The uncertainty increases outside of this region; it is 0.5 % in the vapor phase. The uncertainty in heat capacities is 5 %, and the uncertainty in vapor pressure is 0.1 %. In the gaseous region, the speed of sound can be calculated with an uncertainty of 0.1 %; in the liquid phase, the uncertainty increases to 0.5 %. In the critical region, the uncertainties are higher for all properties except vapor pressure.

5. DISCUSSION AND CONCLUSIONS

We have presented comprehensive and accurate measurements of the $p-\rho-T$ behavior of R1234yf. The measured data cover the largest temperature and pressure region currently available in the open literature. The measured data, when combined with other data types from different sources such as the speed of sound and heat capacity, form a reliable basis to develop a new equation of state. The equation covers liquid, vapor, and supercritical states, and it is suitable for studying refrigeration processes. It has been incorporated into the NIST REFPROP database.[25]

The upper limit of the temperature and the pressure of the current measurements was set to 400 K and 10 MPa to avoid possible polymerization within the measuring cell. Measurements of R1234yf over larger temperature and pressure ranges are desirable but would require further investigations regarding its thermal and chemical stability.

■ ASSOCIATED CONTENT

Supporting Information. The data tabulations in this paper report only a single measurement at each (T, p) state point. Four or more replicate measurements were made at each state point, and all of the data are included. More details on uncertainties are provided, including the temperature, pressure, density, and combined uncertainties for each measured point. The standard deviation in the measured quantities (that is, a measure of the scatter in the multiple temperature and pressure readings carried out for each density determination) are also reported. This material is available free of charge via the Internet at http://pubs.acs.org.

■ AUTHOR INFORMATION

Corresponding Author

*E-mail: markm@boulder.nist.gov. Fax: +1-303-497-5224.

Present Addresses

[†]Lehrstuhl für Thermodynamik, Ruhr-Universität Bochum, Universitätsstrasse 150, D-44780 Bochum, Germany.

■ ACKNOWLEDGMENT

We thank R. Singh and R. Hulse of Honeywell Inc. for providing the high-purity sample of R1234yf. We thank S. Lago and P.A. Giuliano Albo of Istituto Nazionale di Ricerca Metrologica for providing their speed of sound data prior to publication and R. Akasaka of Kyushu Lutheran College for his assistance in obtaining some of the data measured in Japan. We also thank our NIST colleagues, T. Lovestead, for the chemical analysis of the R1234yf, J. Widegren, for assistance in the stability testing, and A. Kazakov for calculating theoretical c_p^0 values.

■ REFERENCES

(1) Nielsen, O. J.; Javadi, M. S.; Sulbaek, M. P.; Hurley, M. D.; Wallington, T. J.; Singh, R. Atmospheric chemistry of $CF_3CF{=}CH_2$: Kinetics and mechanism of gas-phase reactions with Cl atoms, OH radicals, and O_3. *Chem. Phys. Lett.* **2007**, *439*, 18–22.

(2) Tanaka, K.; Higashi, Y. Thermodynamic properties of HFO-1234yf (2,3,3,3-Tetrafluoropropene). *Int. J. Refrig.* **2010**, *33*, 474–479.

(3) American Society of Heating, Refrigerating and Air-Conditioning Engineers, BSR/ASHRAE Standard 34−2010, *Designation and Safety Classification of Refrigerants and Addendum h to Standard 34−2010*, 2010; available at http://ashrae.org/technology/page/132.

(4) Kleinrahm, R.; Wagner, W. Measurement and correlation of the equilibrium liquid and vapour densities and the vapour pressure along the coexistence curve of methane. *J. Chem. Thermodyn.* **1986**, *18*, 739–760.

(5) Wagner, W.; Kleinrahm, R. Densimeters for very accurate density measurements of fluids over large ranges of temperature, pressure, and density. *Metrologia* **2004**, *41*, S24–S39.

(6) McLinden, M. O.; Lösch-Will, C. Apparatus for wide-ranging, high-accuracy fluid ($p-\rho-T$) measurements based on a compact two-sinker densimeter. *J. Chem. Thermodyn.* **2007**, *39*, 507–530.

(7) Lösch-Will, C. Entwicklung und Aufbau neuer Dichtemessapparaturen auf der Basis von Magnetschwebewaagen. Ph.D. Thesis, Ruhr-Universität Bochum, Germany, 2005.

(8) McLinden, M. O.; Kleinrahm, R.; Wagner, W. Force transmission errors in magnetic suspension densimeters. *Int. J. Thermophys.* **2007**, *28*, 429–448.

(9) Bruno, T. J.; Svoronos, P. D. N. *CRC Handbook of Basic Tables for Chemical Analysis*, 3rd ed.; Taylor and Francis CRC Press: Boca Raton, FL, 2011.

(10) Bruno, T. J.; Svoronos, P. D. N. *CRC Handbook of Fundamental Spectroscopic Correlation Charts*; Taylor and Francis CRC Press: Boca Raton, FL, 2005.

(11) Widegren, J.; Bruno, T. Thermal decomposition kinetics of propylcyclohexane. *Ind. Eng. Chem. Res.* **2009**, *48*, 654–659.

(12) McLinden, M. O. Thermodynamic properties of propane. I. p-ρ-T behavior from 265 to 500 K with pressures to 36 MPa. *J. Chem. Eng. Data* **2009**, *54*, 3181–3191.

(13) Span, R.; Wagner, W. Equations of state for technical applications. I. Simultaneously optimized functional forms for nonpolar and polar fluids. *Int. J. Thermophys.* **2003**, *24*, 1–39.

(14) Di Nicola, C.; Di Nicola, G.; Pacetti, M.; Polonara, F. P-V-T behavior of 2,3,3,3-tetrafluoroprop-1-ene (HFO-1234yf) in the vapor phase from (243 to 373) K. *J. Chem. Eng. Data* **2010**, *55*, 3302–3306.

(15) Tanaka, K.; Higashi, Y.; Akasaka, R. Measurements of the isobaric specific heat capacity and density for HFO-1234yf in the liquid state. *J. Chem. Eng. Data* **2010**, *55*, 901–903.

(16) Di Nicola, G.; Polonara, F.; Santori, G. Saturated pressure measurements of 2,3,3,3-tetrafluoroprop-1-ene (HFO-1234yf). *J. Chem. Eng. Data* **2010**, *55*, 201–204.

(17) Lago, S.; Giuliano Albo, P. A.; Brignolo, S. Speed of sound results in 2,3,3,3-tetrafluoropropene (R-1234yf) and trans-1,3,3,3-tetrafluoropropene (R-1234ze(E)) in the temperature range of (260 to 360) K. *J. Chem. Eng. Data* **2011**, *56*, 161–163.

(18) Kano, Y.; Kayukawa, Y.; Fujii, K.; Sato, H. Ideal gas heat capacity for 2,3,3,3-tetrafluoropropene (HFO-1234yf) determined from speed-of-sound measurements. *Int. J. Thermophys.* **2010**, *31*, 2051–2058.

(19) Hulse, R.; Singh, R.; Pham, H. Physical properties of HFO-1234yf. *Proceedings of the 3rd IIR Conference on Thermophysical Properties and Transfer Processes of Refrigerants*, paper 178, Boulder, CO, 2009.

(20) Kazakov, A. National Institute of Standards and Technology, Boulder, CO, private communication, 2010.

(21) Mohr, P. J.; Taylor, B. N.; Newell, D. B. CODATA recommended values of the fundamental physical constants: 2006. *Rev. Mod. Phys.* **2008**, *80*, 633–730.

(22) Lemmon, E. W.; McLinden, M. O.; Wagner, W. Thermodynamic properties of propane. III. A reference equation of state for temperatures from the melting line to 650 K and pressures up to 1000 MPa. *J. Chem. Eng. Data* **2009**, *54*, 3141–3180.

(23) Fedele, L.; Bobbo, S.; Groppo, F.; Brown, J. S.; Zilio, C. Saturated pressure measurements of 2,3,3,3-tetrafluoroprop-1-ene (R1234yf) for reduced temperatures ranging from 0.67 to 0.93. *J. Chem. Eng. Data* **2011**, *56*, 2608–2612.

(24) Yoshitake, M.; Matsuo, S.; Sotani, T. Density and speed of sound measurements of HFO1234yf. *Proceedings of the 30th Japan Symposium on Thermophysical Properties*, Yonezawa, Japan, 2009 (in Japanese).

(25) Lemmon, E. W.; Huber, M. L.; McLinden, M. O. *NIST Standard Reference Database 23, NIST Reference Fluid Thermodynamic and Transport Properties—REFPROP, version 9.0*, Standard Reference Data Program; National Institute of Standards and Technology: Gaithersburg, MD, 2010.